Journal of Anatolian Environmental and Animal Sciences
(*Anadolu Çevre ve Hayvancılık Bilimleri Dergisi*)
DOI: https://doi.org/10.35229/jaes.1421336

JAES
Year: 9, No: 2, 2024 (174-183)
AÇEH
Yıl: 9, Sayı: 2, 2024 (174-183)

ARAŞTIRMA MAKALESİ RESEARCH PAPER

Biogenic Iron Oxide Nanoparticles Based on Algal Biofilm Formed in the Wastewater Treatment Plant and Their Dye Removal Performance [*]

İlyas Taner DEMİREL[1] Bulent AKAR[2]* Cemalettin BALTACI[2]
Omer KARPUZ[3] Esma GÜLBAHAR ERDOĞDU[1]

[1] *Gümüşhane University, Graduate Education Institute, Department of Biotechnology, Gümüşhane, 29000, Türkiye*
[2] *Gümüşhane University, Faculty of Engineering and Natural Sciences, Department of Food Engineering, Gümüşhane, 29000, Türkiye*
[3] *Gümüşhane University, Faculty of Engineering and Natural Sciences, Department of Genetic and Bioengineering, Gümüşhane, 29000, Türkiye*

Received: *22.01.2024* ***Accepted:*** *18.03.2024* ***Puplished:*** *30.06.2024*

How to cite: **Demirel, İ.T., Akar, B., Baltaci, C., Karpuz, O. & Gülbahar, E. (2024).** Biogenic iron oxide nanoparticles based on algal biofilm formed in the wastewater treatment plant and their dye removal performance. *J. Anatolian Env. and Anim. Sciences*, ***9***(2), 174-183. https://doi.org/10.35229/jaes.1421336

Atıf yapmak için: **Demirel, İ.T., Akar, B., Baltaci, C., Karpuz, O. & Gülbahar, E. (2024).** Atıksu arıtma tesisinde oluşan algal biyofilm kökenli biyojenik demir nanopartiküller ve boya giderim performansları. *Anadolu Çev. ve Hay. Dergisi*, ***9***(2), 174-183. https://doi.org/10.35229/jaes.1421336

*: https://orcid.org/0000-0002-1421-374X
: https://orcid.org/0000-0002-8417-8943
: https://orcid.org/0000-0002-4336-4002
: https://orcid.org/0000-0002-0546-9831
: https://orcid.org/0000-0002-3410-8357

***Corresponding author's:**
Bulent AKAR
Gümüşhane University, Faculty of Engineering and Natural Sciences, Department of Food Engineering, Gümüşhane, 29000, Türkiye
✉: akarblnt@gmail.com

Abstract: In the field of environmental pollution removal, bioremediation plays a crucial role in removing or converting toxic substances from the environment. Bacteria, yeasts, molds, algae, and plants are widely used in bioremediation events. Recently, green-synthesized nanoparticles have also been employed in bioremediation applications. In this study, iron oxide nanoparticles (AB-FeONPs) were synthesized from algal biofilms that are naturally formed in the settling ponds of the Gumushane Municipality Wastewater Treatment Plant. These biological nanoparticles were utilized to investigate their adsorption efficiency for water-polluting dyes such as methylene blue (MB), malachite green (MG), and phenol red (PR). The synthesized AB-FeONPs were characterized using Fourier transform infrared spectroscopy (FTIR), scanning electron microscopy (SEM), energy-dispersive X-ray spectrometry (EDX), and X-ray diffraction (XRD). To test their efficacy, MB, MG, and PR dye solutions were treated with 5.0, 10.0, and 20 g/L AB-FeONP concentrations.
In the presence of 20.0 g/L adsorbent, the adsorption percentages for 50 mg/L amounts of MB, MG and PR were 50.22%, 60.43% and 82.71%, respectively. The remaining dye concentrations were quantified with a UV-VIS spectrophotometer after filtration. The results showed that AB-FeONPs effectively removed MB, MG, and PR, with the highest efficiency observed for PR.

Keywords: Algal biofilm; wastewater; iron oxide nanoparticle; dye adsorption.

Atıksu Arıtma Tesisinde Oluşan Algal Biyofilm Kökenli Biyojenik Demir Nanopartiküller ve Boya Giderim Performansları

***Sorumlu yazar:**
Bülent AKAR
Gümüşhane Üniversitesi, Mühendislik ve Doğa Bilimleri Fakültesi, Gıda Mühendisliği Bölümü, Gümüşhane, 29000, Türkiye
✉: akarblnt@gmail.com

Öz: Çevre kirliliği giderimi çalışmalarında biyoremediasyon, toksik maddelerin çevreden uzaklaştırılmasında veya dönüştürülmesinde çok önemli bir rol oynamaktadır. Bakteriler, mayalar, küfler, algler ve bitkiler biyoremediasyonda yaygın olarak kullanılmaktadır. Son zamanlarda, yeşil sentezle elde edilmiş nanopartiküller de biyoremediasyon uygulamalarında tercih edilmektedir. Bu çalışmada, Gümüşhane Belediyesi Atıksu Arıtma Tesisi çökeltme havuzlarında doğal olarak oluşan alg biyofilmlerinden demir oksit nanopartikülleri (AB-FeONP'ler) sentezlenmiştir. Bu biyolojik nanopartiküller, metilen mavisi (MB), malaşit yeşili (MG) ve fenol kırmızısı (PR) gibi suyu kirleten boyaların adsorpsiyon verimliliklerini araştırmak için kullanılmıştır. Sentezlenen AB-FeONP'ler, Fourier dönüşümü kızılötesi spektroskopisi (FTIR) taramalı elektron mikroskobu (SEM), enerji dağılımlı X-ışını spektrometrisi (EDX) ve X-ışını kırınımı (XRD) kullanılarak karakterize edilmiştir. AB-FeONP'lerin etkinliklerini test etmek için MB, MG ve PR boya çözeltileri 5.0, 10.0 ve 20 g/L AB-FeONP konsantrasyonları ile muamele edilmiştir. 20.0 g/L adsorban varlığında, MB, MG ve PR'nin 50 mg/L miktarları için adsorpsiyon yüzdeleri sırasıyla %50,22, %60,43 ve %82,71 olmuştur. Kalan boya konsantrasyonları filtrasyondan sonra UV-VIS spektrofotometre ile ölçülmüştür. Sonuçlar, AB-FeONP'lerin MB, MG ve PR'yi etkili bir şekilde ortadan kaldırdığını ve en yüksek verimliliğin PR'de elde edildiğini göstermiştir.

Anahtar kelimeler: Algal biyofilm; atıksu; demir oksit nanopartikül; boya adsorpsiyonu.

[*] *This study was produced from the master thesis of the İlyas Taner DEMİREL.*

INTRODUCTION

It is vital to adequately protect and restore the planet's ecological integrity to ensure the continuity of critical life support systems (Westra et al., 2000). There has been a serious increase in the accumulation of polluting substances in the environment since the Industrial Revolution (Naidu et al., 2021). Studies on treatment strategies such as bioremediation and physicochemicals have become more popular in recent years due to rising environmental challenges. Bioremediation is an eco-friendly and sustainable technology used for environmental management (Azubuike 2020). It involves using organisms like bacteria, algae, fungi, and plants to remove or transform toxic substances that cause environmental pollution in their accumulation areas (Chekroun, 2014; Vazquez-Nunez et al., 2020). Scientists have been developing new applications and methods to increase the effectiveness of bioremediation. Nanotechnology is a rapidly growing field that has found its way into various commercial and domestic applications. It is used in catalysis, imaging, medical research, energy-based research, and environmental fields (Khan et al., 2019; Khan et al., 2022). Although bioremediation is an effective and flexible recovery strategy for pollutants, it is limited to high concentrations of pollutants and refractory compounds, making it unsustainable alone. Nanoparticle application in indirect bioremediation can be considered an innovative strategy to carry environmental remediation beyond these limits (Kumar and Gopinath, 2017; Vazquez-Nunez et al., 2020). Although traditional nanotechnology applications depend on chemical and physical techniques, these applications are considered disadvantageous due to their toxicity to the environment and are expensive. New biotechnological approaches, on the other hand, use biomolecules (green synthesis) found in microorganisms, algae, or higher vascular (having delivery systems) and non-vascular plants to produce nanoparticles of desired shape and size that mimic nature (Tripathi et al., 2022). Algae with phototrophic organisms with eukaryotic and prokaryotic cell structures are the primary producers of aquatic ecosystems (seas, oceans, lakes, and streams) covering 71% of the world's surface (Andersen, 1992; Akar et al., 2019). They grow not only in aquatic ecosystems but also in extreme conditions such as dry, cold, and hot terrestrial habitats and develop on animals and plants in places with little light, up to a few centimeters deep in the soil, on snow and ice masses (Hofmann 1989). They adapt well to these extreme environmental conditions by synthesizing many natural compounds called secondary metabolites (Akar et al., 2019; Shah et al., 2020). Algae are used in many areas of industry (food, cosmetics, pharmaceuticals, and medicine) due to their rich chemical composition and content of bioactive substances. Products derived from them, such as agar, alginate, and carrageenan, are used as gelling, thickening, and stabilizing agents (Scieszka and Klewicka 2019). Recently, researchers have pointed out that algae represent an important potential source of bioactive compounds (Plaza et al., 2010, Amlani and Yetgin, 2022). Algae contain various bioactive compounds, including polyphenols, flavonoids, amino acids, lignins, terpenoids, tocopherols, fatty acids, and phenolic acids (Akar et al., 2019). Algae have a high diversity of these compounds, bringing them to the forefront of nanoparticle synthesis with green synthesis. Because these bioactive compounds have the capacity to convert metal ions into metal nanoparticles with a simple application at room temperature (Ebrahiminezhad et al., 2018), Algae are able to accumulate metals and reduce metal ions; this feature has made them competitive with other organisms for the biosynthesis of nanoparticles. Furthermore, algae have many other advantages, such as higher energy efficiency, low-temperature synthesis with less toxicity to the environment, and being relatively convenient and easy to use (Lewis Oscar et al., 2016). Algae in aquatic ecosystems grow as benthic (attached to a surface) or planktonic (free in water). Additionally, benthic algae and other microorganisms form an algal biofilm, a complex community (dominated by algae) growing on solid surfaces such as submerged stones and pebbles, rivers, wet wall surfaces, and tree bark. Algal biofilms are layers of extracellular polymeric substances in a matrix. (Kesaano and Sims, 2014; Thapa et al., 2017). Although algae biofilms are known to cause both safety and economic problems due to their dense formation on structures (Leadbeater and Callow 1992), they are seen as an important material for applications such as wastewater remediation, nutrient control, efficient, low-cost biomass harvesting techniques, and alternative biofuel stock-building strategies in recent years (Kesaano and Sims 2014; Thapa et al., 2017). Dyes in wastewater from various industries cause high organic loads and color formation, making them an important class of pollutants. Removing pollutants is necessary before discharging wastewater into the environment (Saravanan et al., 2021). Traditional dye removal methods are costly and difficult to use. In recent decades, nanotechnology has received considerable interest due to the fast and effective removal of dyes accomplished through nanoparticles (Badawi et al., 2021). This study aimed to characterize iron oxide nanoparticles obtained from algal biofilms, which are naturally and continuously formed in the sedimentation ponds where the treated water is in the Gumushane Municipality Wastewater Treatment Plant, and to reveal their potential in the removal of polluting organic dyes such as methylene blue (MB), malachite green (MG) and phenol red (PR) from water.

MATERIAL AND METHOD

Sampling: Algal biofilm samples on the metal plates were collected in 2022 by scraping from the surface using a spatula. Then, the samples were washed with distilled water and dried at room temperature.

Extraction: Dried algal biofilm samples were ground into powder using a blender. Then, 200 g of the powdered sample was taken, completed with distilled water to 2000 mL, and then boiled for 60 min under a reflux cooler. These samples were cooled and filtered with ordinary filter paper to obtain the algal extract. After the formation of the extract, it was allowed to cool and filtered through sieves with pore sizes of 2.00 mm, 1.00 mm, and 0.25 mm, respectively. The dry matter content of the sieved extract was then determined by a digital refractometer (Hanna HI96801, Hanna Instruments, Milan, Italy). As a result of the analysis, the dry matter content of the algal extract was determined to be 4.00±0.25%. The dry matter content was then increased to 10% using a vacuum evaporator at 60 ºC under 150 mbar pressure (Karakullukçu et al., 2023; Gedikli et al., 2024).

Preparation of AB-FeONPs: First, 0.2 M Fe^{+3} and Fe^{+2} solution, $FeCl_3.6\ H_2O$/1.9 g $FeSO_4$ solution, and algal extracts were added in a ratio of 1:1, v/v, and mixed at room temperature on a magnetic stirrer for 1 h. It was checked whether a black precipitate appeared, indicating that Fe^{2+} ions were reduced. The AB-FeONPs were allowed to dry in a vacuum oven set at 65 °C for 3 hours (Yusefi et al., 2020; Gedikli, 2024).

Characterization of AB-FeONPs: FTIR, SEM, and XRD analyses were performed at Ataturk University East Anatolia High Technology Application and Research Center. FTIR measurements were performed on a Bruker VERTEX 70v device (Bruker Optik GmbH, Rosenheim, Germany) using the Opus program in the range of 400–4000 as absorbance 32 times with a sensitivity of 4 cm^{-1}. EDX elemental analysis and SEM images of synthesized AB-FeONPs were obtained using SEM (SEM-Zeiss Sigma 300, Carl Zeiss AG, Oberkochen, Germany). The diameters and size distribution of nanoparticles were determined by measuring over 100 nanoparticles using the ImageJ software program (Rueden et al., 2021) through acquired SEM images. XRD analysis was performed through the PANalytical Empyrean XRD (Empyrean, Almelo, The Netherlands) at 45 kV and 40 mA with a scan rate of 0.05 degrees\second.

Determination of dye removal efficiency of FeONP: Methylene blue, malachite green, and phenol red dyes were used in the study. Their structures are shown in Figure 1. Stock solutions of MB, MG, and PR were prepared at a 2500.0 mg/L concentration. From these stock solutions, dilutions were made at appropriate ratios, and six consecutive dye solutions (1.0, 2.5, 5.0, 10.0, 25.0, 50.0, 100.0, and 250.0 mg/L) between 1.0 and 250.0 mg/L were prepared. The pH of these prepared dye solutions were as 4.87 for MB, 3.01 for MG, and 3.75 for PR.

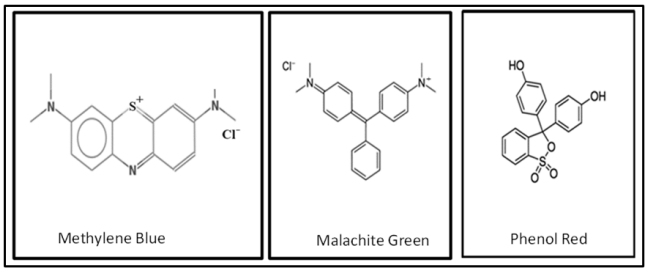

Figure 1. Chemical structures of the dyes.

Then. 0.05, 0.100, and 0.200 g of AB-FeONP were transferred into polypropylene tubes, and 10 mL each of dye solutions ranging from 1.0–250.0 mg/L were added separately. In addition, 10 mL of pure water was added to 0.050 and 0.100 g of AB-FeONPs for blind reading in the spectrophotometer. The mixtures were placed in a shaker and incubated at a shaking frequency of 50 rpm for 12 hours at room temperature. During the preliminary studies on the adsorption of nanoparticles, it was observed that the rate of adsorption reached a steady state after 8 hours. Therefore, a duration of 12 hours was selected for the adsorption process. Then, the solutions were filtered through a 0.45 µm nitrocellulose membrane, and the concentrations of un-adsorbed dyes in the filtrate were measured using UV-VIS spectrophotometry (Shimadzu UV-1800, Kyoto, Japan) (Bozbeyoglu et al., 2020). Spectrum scanning was conducted for MB using a 5.0 mg/L solution in a spectrophotometer at 200–1000 nm wavelengths. A wavelength of 664 nm was determined to provide the highest absorbance level. Calibration graphs were plotted at five varied concentrations of 1.0, 2.5, 5.0, 10.0, and 25.0 mg/L. The procedures were carried out identically for MG and PR, resulting in maximum absorbance values of 617 and 430, respectively. The concentrations of the remaining dyes in the solution were calculated using the calibration graph equations, as specified in Equation 1 (Bozbeyoglu et al., 2020).

$$Remaining\ dye\ \left(\frac{mg}{L}\right) = (A - B)/E \quad (1)$$

In equation 1, A is the absorbance, b is the y-intercept, and E is the slope. Equation 2 (Bozbeyoglu et al., 2020) was used to calculate the adsorption percentage.

$$Adsorption\ Percentage = ((C_o - C_e)/C_o)\ x\ 100 \quad (2)$$

In equation 2, the initial concentration of the adsorbent is denoted by C_o (mg/L), while Ce (mg/L) represents the quantity of adsorbent remaining un-adsorbed in the equilibrium solution. All experiments were conducted

in triplicate. The results are presented in mean and standard deviation values.

Equation 3 was used to determine the adsorption capacity, which indicates the amount of dye adsorbed per gram of AB-FeONPs, based on the concentration of the unadsorbed adsorbent.

$$Qe = \ ((Co - Ce)\ x\ V)/m \quad (3)$$

Qe: Quantity of dye retained by 1 g AB-FeONPs (mg/g); Co: Initial adsorbent concentration (mg/L); Ce: Unadsorbed adsorbent concentration in equilibrium solution (mg/L); m: Adsorbent amount (g); V: Adsorbent volume (mL) (Bozbeyoglu et al. 2020).

RESULTS AND DISCUSSION

Characterization of AB-FeONPs: During the synthesis of the nanoparticles. with algal biofilm extraction, the solution's discoloration to black demonstrates that AB-FeONPs have been produced. SEM images of AB-FeONPs obtained using algal biofilm are presented in Figure 2 at 50.00 KX and 80.00 KX magnification (Figure 2). The determination of nanoparticles' diameters and their size distribution was performed using ImageJ software after acquiring the SEM images (Figure 3). The nanoparticles were homogenously spherical-shaped, and the nanoparticle sizes were well distributed; they were measured between 13.96 and 38.13 nm. The average size of the measured AB-FeONPs is 23.40 nm (Figure 3).

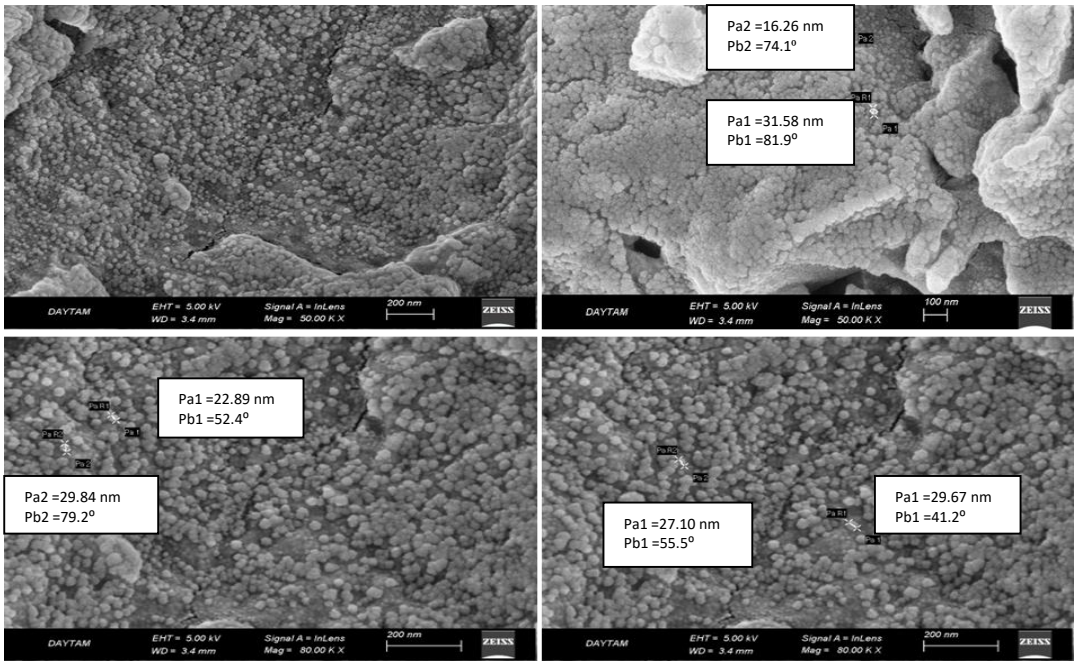

Figure 2. SEM images of AB-FeONPs.

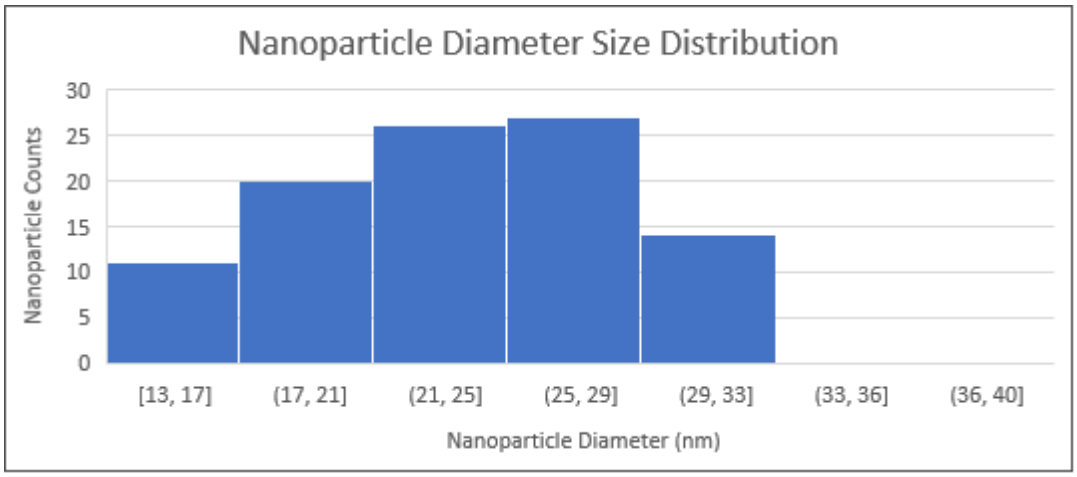

Figure 3. Diameter size distribution of AB-FeONPs via imageJ software.

Elemental analysis of a sample is accomplished by collecting characteristic X-rays, which are produced while scanning the sample with electron beams (Shojaei et al., 2022). EDX is used to obtain rapid analysis of elements. The spectrum acquired from EDX analyses of AB-FeONPs is shown in Figure 4, and the quantitative

results are given in Table 1. The examined elements comprise carbon (C), oxygen (O), and iron (Fe). The positions of the peaks were used to identify the elements, and the height of the peaks made it possible to quantify the concentration of each element. A high percentage of oxygen can be considered evidence that the nanoparticles are in the form of iron oxide (Demirezen et al., 2019).

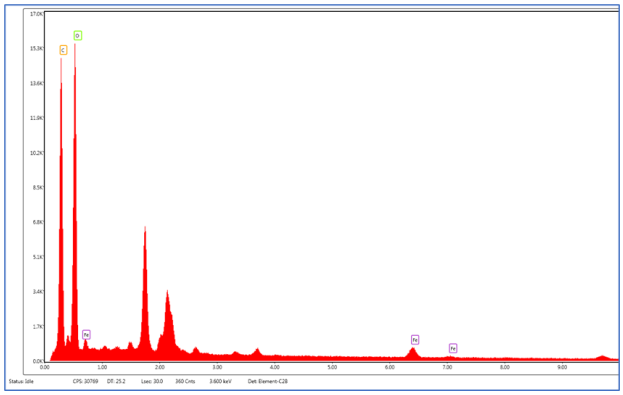

Figure 4. EDX spectrum of AB-FeONPs.

The weight percentages of oxygen, carbon, and iron in AB-FeONPs have been determined to be 50.55%, 40.79%, and 8.65%, respectively. Karakullukçu et al. (2023) found that the oxygen, carbon, and iron weight percentages of iron oxide nanoparticles derived from firethorn fruits were 47.33%, 38.46%, and 14.21%, respectively. Additionally, the percentages of carbon, oxygen, and iron atoms were determined to be 49.92%, 46.11%, and 3.97%, correspondingly. Jain et al. (2021) reported the weight percentages of elements as 54.23% C, 29.27% O, 1.25% Cl, and 15.25% Fe in the EDX analysis of iron oxide nanoparticles obtained from the peel of jack fruit *(Artocarpus heterophyllus* Lam., Encycl.*).*

Table 1. EDX analysis of AB-FeONPs

Element	% Weight	% Atom
C	40.79	50.61
O	50.55	47.08
Fe	8.65	2.31

FTIR identified possible phenolic compounds that may be responsible for the conjugation and reduction of iron oxide nanoparticles synthesized using algal biofilm extract. The FTIR analysis spectra of the extract from the algal biofilm and AB-FeONPs are presented in Figure 5. Various vibrational bands observed in the spectrum of biomolecules in the 400–4000 cm^{-1} range reveal that functional groups are accountable for the reduction of iron in biomolecules presenting with capping and reducing properties. The findings from conducting FTIR analysis reveal O-H stretching vibrations of adsorption C-OH and H_2O groups at a frequency of 3300 cm^{-1}. Peaks at 2920–2950 cm^{-1} correspond to the stretching vibration of the methyl and methylene groups of C-H. Peaks at 1635 and 1035 cm^{-1} indicate the presence of carbonyl groups (C=O) and C-O single bonds, respectively. Other peaks at 1635 and 1035 cm^{-1} correspond to carbonyl groups (C=O) and C-O single bonds, respectively. The peak observed at 1635 cm^{-1} is attributed to the C=O vibration that may be related to conjugated ketones, quinones, carboxylic acids, and esters (Carballo et al., 2008). This peak also indicates the C=C stretching. Furthermore, bands appearing at 1635, 1542, 1421, and 1392 cm^{-1} suggest the presence of alkenes and aromatic structures. The peak at approximately 1400 cm^{-1} indicates the presence of an aromatic structure and shows polyphenolic O-H bending (typical of hydroxyl groups, phenolic hydroxyl). The peaks at 870 cm^{-1} and 668 cm^{-1} in the spectrum indicate CH bending, and they are an example of the heterocyclic compounds derived from flavonoids and alkaloids found in the plant extract mentioned earlier (Alsammarraie et al., 2018). FTIR analysis of extracts from algal biofilm and AB-FeONPs showed the distinctive absorption peaks of various biomolecules. The data indicates a close correlation between the two spectrums, supporting the idea that AB-FeONPs may be potentially used in green energy production.

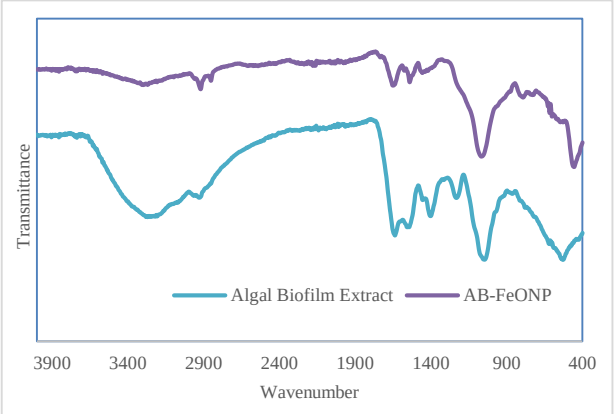

Figure 5. FTIR spectrums of extract from algal biofilm and AB-FeONPs.

The XRD spectrum for AB-FeONPs, synthesized using the green method, is shown in Figure 6. A total of 5 peaks were detected in the 2θ range of 20–70°, and their planes were determined to be 30.75 (220), 36.05 (311), 43.90 (400), and 57.7 (511). X-ray diffraction results conform to the pure cubic spinel structure of magnetite (JCPDS card number: 19–629) (Berger et al., 1999; Wang et al., 2002; Gong and Lin, 2003). As detected in a study on green tea waste (Fan et al., 2017), the peaks of AB-FeONPs at 22° and 26° are thought to originate from amorphous organic compounds obtained from algae extracts as a stabilizing agent through AB-FeONPs. Peaks at 29.49, which point to the detection of some impurities corresponding to the γ-FeOOH phase, were also reported (Golshahi et al., 2018). While the cubic spinel structure can contain both magnetite and maghemite phases and exhibit the same XRD patterns, the black color of the NPs also

indicated that the nanoparticles contained the magnetite phase and did not contain the maghemite phase (brown color) (Abbas et al., 2017).

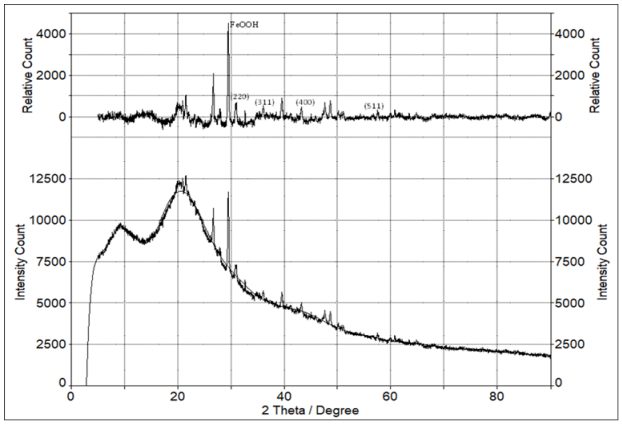

Figure 6. XRD patterns of the AB-FeONPs.

Determination of dye removal efficiency of FeONP: The amount of dye remaining and the percentages of adsorption at different concentrations of each dye were presented in Table 2. In addition, Co, Ce, and Qe adsorption percentage values at 5.0 g/L, 10 g/L, and 20 g/L at the adsorbent amounts are shown in Figures 7–9. First, the impact of synthesized Fe-NPs' adsorption activity on different MB concentrations was investigated. Most of the time, industrial wastewater containing dye includes dissolved inorganic ions, which can significantly impact the efficiency of dye adsorption. These ions can compete with the dye for active sites on the adsorbent surface, or they can become inactive inside the adsorbent, which makes the adsorption process less effective overall (Mahdavinia et al., 2013). In this study, only the effect of various concentrations of the adsorbents on dye removal was investigated. The experiments were carried out in three triplicates. As shown in Table 2 and Figure 7-9, as the adsorbent concentration increases, the adsorption percentage also rises. For example, adsorption percentages were calculated 48.12% for 5.0 g/L adsorbent, 65.70% for 10.0 g/L adsorbent, and 88.64% for 20 g/L adsorbent in the 1.0 mg/L solution of MB. The amount of nanoparticles used in the adsorption process is directly linked to the removal of the dye. Higher nanoparticle doses increase the adsorbent surface area and the accessibility of additional free active binding sites, enhancing adsorption. However, increasing the dosage does not significantly increase adsorption after a certain point due to the agglomeration of nanoparticles and saturation of adsorption sites. Some researchers have also suggested that the equilibrium adsorption state may increase at high nanoparticle dosages due to intermolecular competition (Arabi and Sohrabi 2014). Hamdy et al. (2018) reported that increasing the dose of nanoparticles from 2 to 10 g/L resulted in a higher MB removal efficiency, from 85.4% to 97.5%. It can be explained that the abundance of active sites on the surface of the nanoparticles is responsible for their high adsorption capability at lower concentrations of dye (Nwodika and Onukwuli 2017). However, when AB-FeONP was used as an adsorbent at 20.0 g/L, the adsorption percentage was 88.64% in the 1.0 mg/L solution of MB, while this value decreased to 33.32% in the 250.0 mg/L solution (Table 2, Figure 9). While the percentage of MB and MG adsorption increases with a higher amount of adsorbent, the amount of MB and MG adsorbed per gram of adsorbent decreases. This situation can be attributed to two factors. First, at a constant MB concentration, the amount of adsorbent increases, resulting in numerous active sites on the adsorbent surface for unsaturated adsorption. Also, the agglomeration of large numbers of adsorbent particles reduces the total surface area, thereby reducing the adsorption capacity of the adsorbent (Sulaiman et al., 2021). In MG dye removal experiments, the adsorption percentage increased as the adsorbent concentration increased.

Table 2: MB adsorption rates of AB-FeONPs at different concentration.

C_0 mg/L	Dye	5.0 g/L C_e mg/L	10.0 g/L C_e mg/L	20.0 g/L C_e mg/L	5.0 g/L % Ads.	10.0 g/L % Ads.	20.0 g/L % Ads.
	MB	0.52±0.03	0.34±0.07	0.11±0.04	48.12±3.30	65.70±4.75	88.64±3.71
1.0	MG	0.11±0.03	0.06±0.02	0.00±0.00	89.13±0.23	93.96±2.09	100.00±0.00
	PR	0.00±0.00	0.00±0.00	0.00±0.00	100.00±0.00	100.00±0.00	100.00±0.00
	MB	1.57±0.08	1.10±0.03	0.70±0.06	37.06±3.27	55.84±1.32	71.96±2.32
2.5	MG	0.64±0.02	0.58±0.18	0.00±0.00	74.40±0.84	76.81±7.25	100.00±0.00
	PR	0.01±0.01	0.33±0.04	0.00± 0.00	94.30±9.31	86.77±1.61	100.00±0.00
	MB	3.26±0.21	2.54±0.02	1.84±0.08	34.83±4.18	49.24±0.39	63.17±1.59
5.0	MG	1.97±0.09	1.65±0.08	1.16±0.03	60.63±1.82	66.91±1.51	76.81±0.65
	PR	1.34±0.45	0.98±0.14	0.00±0.00	71.34±3.26	80.48±2.79	100.00±0.00
	MB	6.90±0.05	6.33±0.20	4.38±0.05	30.95±0.52	36.74±1.96	56.21±0.50
10.0	MG	4.57± 0.19	4.44±0.21	3.09±0.04	54.35±1.92	55.56±2.09	69.08±0.42
	PR	3.56±0.78	2.72±0.21	0.83±0.04	66.05±1.45	72.77±2.07	91.67±0.36
	MB	18.06±0.64	16.87±0.01	11.88±0.33	27.77±2.57	32.50±0.30	52.50±1.32
25.0	MG	14.99±0.24	14.84±0.18	9.09±0.78	40.05±0.96	40.63±0.71	63.62±0.54
	PR	9.97±0.89	7.02±0.04	3.07±0.08	60.34±0.67	71.90±0.16	87.73±0.33
	MB	39.58±0.20	35.46±0.02	24.89±0.73	20.85±0.41	29.08±0.02	50.22±1.45
50.0	MG	34.67±0.12	33.01±0.36	19.78±0.67	30.65±0.03	33.99±0.72	60.43±0.87
	PR	23.11±0.65	16.97±0.08	8.65±0.08	54.02±0.42	66.06±0.17	82.71±0.17
	MB	79.41±0.39	75.09±0.10	62.19±0.59	20.59±0.39	24.91±0.10	37.81±0.59
100.0	MG	73.93±0.02	68.01±0.04	40.72±0.36	26.07±0.02	31.99±0.04	59.28±0.36
	PR	49.36±0.34	35.17±0.12	19.35±0.19	50.50±0.23	64.83±0.12	80.65±0.19
	MB	209.24±0.77	195.61±0.81	166.71±0.47	16.30±0.31	21.76±0.33	33.32±0.19
250.0	MG	191.81±0.50	175.40±2.51	108.51±0.34	23.28±0.20	29.84±1.00	56.59±0.43
	PR	125.65±0.45	92.58±0.05	54.01±0.02	49.79±0.09	62.97±0.02	78.40±0.01

Ads: Adsorption

However, at the maximum absorbent concentration, there was a decrease in the percentage of adsorption as the concentration of the dye solution increased. For instance, at a concentration of 20.0 g/L, AB-

FeONP was capable of adsorbing 100.00% of MG in a 1.0 mg/L solution, but at a concentration of 250.0 mg/L, the adsorption percentage was reduced to 56.59% (Table 2, Figure 9). In a study on removal dye, it has been reported that increasing the amount of iron oxide nanoparticles in a 50 mL dye solution (50 mg/L) from 0.01 to 0.04 g resulted in the complete removal of brilliant green and MB dyes, with removal rates increasing from 73.8% to 100% and from 94.3% to 100%, respectively (Joshi et al., 2019).

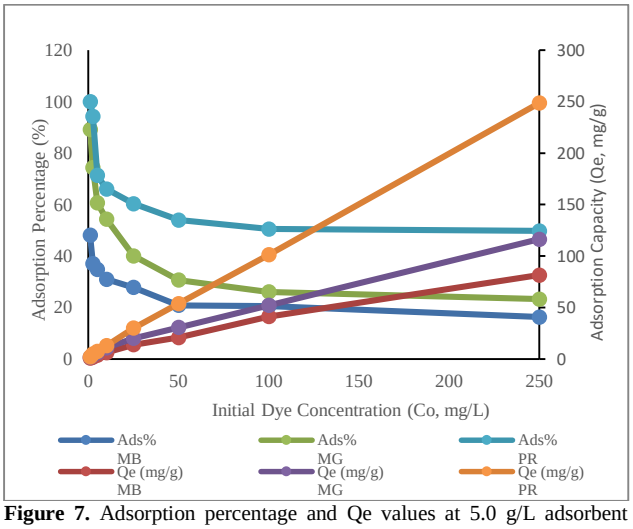

Figure 7. Adsorption percentage and Qe values at 5.0 g/L adsorbent amount.

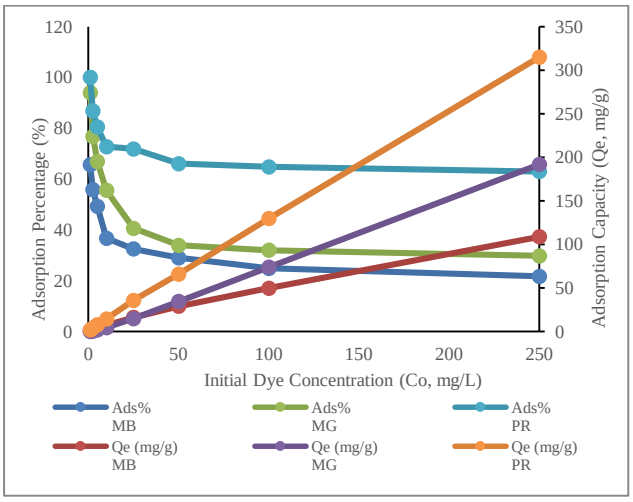

Figure 8. Adsorption percentage and Qe values at 10.0 g/L adsorbent amount.

The results of the adsorption of different concentrations of PR at selected doses of AB-FeONPs are given in Table 2. As seen with other dyes, an increase in the adsorbent concentration is observed to increase the adsorption percentage for PR dye. According to the results (Table 2, Figures 7–9), AB-FeONP had higher adsorption rates for PR than MG and MB. The results can be explained by the presence of different functional groups within the substances. When the chemical structures of all three dyes are evaluated (Figure 1), there are five oxygens in PR. The superior adsorption of PR can be attributed to the electronegative oxygen atom, in contrast to the sulfur and nitrogen atoms. Furthermore, the dyes' adsorption capacity may be influenced by the molecules' three-dimensional spatial configuration.

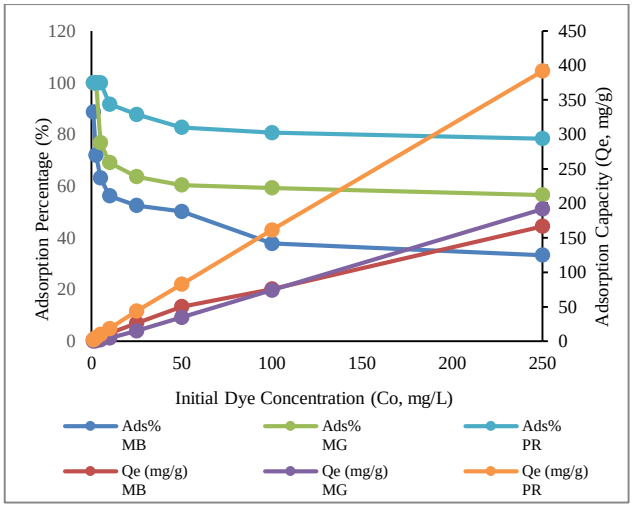

Figure 9. Adsorption percentage and Qe values at a 20.0 g/L adsorbent amount.

CONCLUSION

The study aimed to investigate the green synthesis of iron oxide nanoparticles using algal biofilm and their potential for remediating various dyes. SEM images showed that NPs were present at the nanoscale, while EDX images indicated that iron and oxygen originated from Fe_3O_4. The presence of carbon suggested the presence of organic compounds. FTIR analyses of the algal biofilm extract and AB-FeONPs showed that polyphenols acted as reducing and capping agents. These agents reduce the aggregation of AB-FeONPs, improve their stability, and, hence, reactivity. XRD analysis of AB-FeONPs showed the characteristic peaks of Fe_3O_4. Metal nanoparticles are potential agents for effectively and efficiently removing dyes from wastewater, even at low adsorbent concentrations. AB-FeONPs are the most cost-effective among different types of metal nanoparticles with their high catalytic activity, easy synthesis, and high intrinsic reactivity. They can be used effectively as an adsorbent and degrader for rapidly removing harmful dyes from the aqueous phase. In this study, AB-FeONPs showed efficiency in removing MB, MG, and PR. The highest removal performance was observed in PR elimination.

REFERENCES

Abbas, M., Rao, B.P., Naga, S.M., Takahashi, M. & Kim, C. (2013). Synthesis of high magnetization hydrophilic magnetite (Fe_3O_4) nanoparticles in single reaction-surfactantless polyol process. *Ceramics International*, ***39***(7), 7605-7611. DOI: 10.1016/j.ceramint.2013.03.015

Akar, B., Akar, Z. & Şahin, B. (2019). Identification of antioxidant activity by different methods of a freshwater alga *Microspora* sp. collected from a

high mountain lake. *Hittite Journal of Science and Engineering*, ***6***(1), 25-29. DOI: 10.17350/HJSE19030000129

Alsammarraie, F. K., Wang, W., Zhou, P., Mustapha, A. & Lin, M. (2018). Green synthesis of silver nanoparticles using turmeric extracts and investigation of their antibacterial activities. *Colloids and Surfaces B: Biointerfaces*, ***171***, 398-405. DOI: 10.1016/j.colsurfb.2018.07.059

Amlani, M., & Yetgin, S. (2022). Seaweeds: Bioactive components and properties, potential risk factors, uses, extraction and purification methods. *Marine Science and Technology Bulletin*, ***11***(1), 9-31.

Andersen, R.A. (1992). Diversity of eukaryotic algae. *Biodiversity and Conservation*, ***1***, 267-292. DOI: 10.1007/BF00693765

Arabi, S. & Sohrabi, M., (2014). Removal of methylene blue, a basic dye, from aqueous solutions using nano-zerovalent iron. *Water Science and Technology*. ***70***, 24-31. DOI: 10.2166/wst.2014.189

Azubuike, C.C., Chikere, C.B. & Okpokwasili, G.C. (2020). Bioremediation: An eco-friendly sustainable technology for environmental management. In: Saxena, G., Bharagava, R. (Ed) *Bioremediation of Industrial Waste for Environmental Safety: Volume I: Industrial Waste and Its Management*, 19-39p, Springer, Singapore. DOI: 10.1007/978-981-13-1891-7_2

Badawi, A.K., Abd Elkodous, M. & Ali, G.A. (2021). Recent advances in dye and metal ion removal using efficient adsorbents and novel nano-based materials: an overview. *RSC Advances*, ***11***(58), 36528-36553. DOI: 10.1039/D1RA06892J

Banerjee, S. & Chattopadhyaya, M.C. (2017). Adsorption characteristics for the removal of a toxic dye, tartrazine from aqueous solutions by a low cost agricultural by-product. *Arabian Journal of Chemistry*, ***10,*** 1629-1638. DOI: 10.1016/j.arabjc.2013.06.005

Berger, P., Adelman, N. B., Beckman, K. J., Campbell, D. J., Ellis, A.B. & Lisensky, G.C. (1999). Preparation and properties of an aqueous ferrofluid. *Journal of Chemical Education*, ***76***(7), 943-948. DOI: 10.1021/ed076p943

Bozbeyoglu, P., Duran, C., Baltaci, C. & Gundogdu, A. (2020). Adsorption of Methylene Blue from Aqueous Solution with Sulfuric Acid Activated Corn Cobs: Equilibrium, Kinetics, and Thermodynamics Assessment. *Hittite Journal of Science and Engineering*, ***7***(3), 239-256. DOI: 10.17350/HJSE19030000193

Carballo, T., Gil, M. V., Gómez, X., González-Andrés, F. & Morán, A. (2008). Characterization of different compost extracts using Fourier-transform infrared spectroscopy (FTIR) and thermal analysis. *Biodegradation*, ***19***, 815-830. DOI: 10.1007/s10532-008-9184-4

Chekroun, K.B., Sánchez, E. & Baghour, M. (2014). The role of algae in bioremediation of organic pollutants. *International Research Journal of Public and Environmental Health*, ***1***, 19-32.

Demirezen, D.A., Yıldız, Y.Ş., Yılmaz, Ş. & Yılmaz, D.D. (2019). Green synthesis and characterization of iron oxide nanoparticles using *Ficus carica* (common fig) dried fruit extract. *Journal of Bioscience and Bioengineering*, ***127***(2), 241-245. DOI: 10.1016/j.jbiosc.2018.07.024

Ebrahiminezhad, A., Zare-Hoseinabadi, A., Sarmah, A.K., Taghizadeh, S., Ghasemi, Y. & Berenjian, A. (2018). Plant-mediated synthesis and applications of iron nanoparticles. *Molecular Biotechnology*, ***60***, 154-168. DOI: 10.1007/s12033-017-0053-4

Fan, S., Wang, Y., Li, Y., Tang, J., Wang, Z., Tang, J., Li, X. & Hu, K. (2017). Facile synthesis of tea waste/Fe_3O_4 nanoparticle composite for hexavalent chromium removal from aqueous solution. *RSC Advances*, ***7***(13), 7576-7590. DOI: 10.1039/C6RA27781K

Gedikli, H., Akdogan, A., Karpuz, O., Akmese, O., Kobya, H. N. & Baltaci, C. (2024). Aflatoxin detoxification by biosynthesized iron oxide nanoparticles using green and black tea extracts, *BioResources*, ***19***(1), 380-404. DOI: 10.15376/biores.19.1.380-404

Golshahi, S., Ahangar, A,G., Mir, N. & Ghorbani, M. (2018). A comparison of the use of different sources of nanoscale iron particles on the concentration of micronutrients and plasma membrane stability in sorghum. *Journal of Soil Science and Plant Nutrition*, ***18***(1), 236-252. DOI: 10.4067/S0718-95162018005000902

Gong, J. & Lin, X. (2003). Facilitated electron transfer of hemoglobin embedded in nanosized Fe_3O_4 matrix based on paraffin impregnated graphite electrode and electrochemical catalysis for trichloroacetic acid. *Microchemical Journal*, ***75***(1), 51-57. DOI: 10.1016/S0026-265X(03)00053-5

Hamdy, A., Mostafa, M. K. & Nasr, M. (2018). Zero-valent iron nanoparticles for methylene blue removal from aqueous solutions and textile wastewater treatment, with cost estimation. *Water Science and Technology*, ***78***(2), 367-378. DOI: 10.2166/wst.2018.306

Hoffmann, L. (1989). Algae of terrestrial habitats. *The Botanical Review*, ***55***, 77-105. DOI: 10.1007/BF02858529

Jain, R., Mendiratta, S., Kumar, L. & Srivastava, A. (2021). Green synthesis of iron nanoparticles using Artocarpus heterophyllus peel extract and their application as a heterogeneous Fenton-like catalyst for the degradation of Fuchsin Basic dye. *Current Research in Green and Sustainable Chemistry*, **4**, 100086. DOI: 10.1016/j.crgsc.2021.100086

Joshi, S., Garg, V.K., Kataria, N. & Kadirvelu, K. (2019). Applications of Fe_3O_4@AC nanoparticles for dye removal from simulated wastewater, *Chemosphere*, ***236***, 1-11. DOI: 10.1016/j.chemosphere.2019.07.011

Karakullukcu, V., Akar, B., Baltacı, C., Duzgun, A.O. & Karpuz, O. (2023). Characterization, antioxidant and antimicrobial activities of iron nanoparticles synthesized using firethorn fruit (*Pyracantha coccinea* Roemer) extracts, *Karaelmas Science Journal*, ***13***(2), 255-265. DOI: 10.7212/karaelmasfen.1297963

Kesaano, M. & Sims, R.C. (2014). Algal biofilm based technology for wastewater treatment. *Algal Research*, ***5***, 231-240. DOI: 10.1016/j.algal.2014.02.003

Khan, I., Saeed, K. & Khan, I. (2019). Nanoparticles: Properties, applications and toxicities. *Arabian journal of Chemistry*, ***12***(7), 908-931. DOI: 10.1016/j.arabjc.2017.05.011

Khan, Y., Sadia, H., Ali Shah, S.Z., Khan, M.N., Shah, A.A., Ullah, N., Ullah, M.F. Bibi, H., Bafakeeh, O.T., Khedher, N.B., Eldin, S.M. Fadhl, B.M. & Khan, M.I. (2022). Classification, synthetic, and characterization approaches to nanoparticles, and their applications in various fields of nanotechnology: A review. *Catalysts*, ***12***(11), 1386. DOI: 10.3390/catal12111386

Kumar, S.R. & Gopinath, P. (2017). Nano-bioremediation applications of nanotechnology for bioremediation. In: Wang, L.K., Wang, M.S., Hung, Y.T., Shammas, N.K., Chen,J.P. (Ed), *Handbook of advanced industrial and hazardous wastes management*, 27-48p, CRC Press, New York.

Leadbeater, B.S.C. & Callow, M.E. (1992). Formation, composition and physiology of algal biofilms. In: Melo, L.F., Bott, T.R., Fletcher, M., Capdeville, B. (Ed) *Biofilms-science and technology*, 149-162p. Springer, Netherlands.

Lewis Oscar, F., Vismaya, S., Arunkumar, M., Thajuddin, N., Dhanasekaran, D. & Nithya, C. (2016). Algal nanoparticles: synthesis and biotechnological potentials. In: Thajuddin, N., Dhanasekaran, D. (Ed), *Algae-organisms for imminent biotechnology*, 157-182p. Intechopen, Croatia.

Mahdavinia, G.R., Aghaie, H., Sheykhloie, H., Vardini, M.T. & Etemadi, H. (2013). Synthesis of CarAlg/MMt nanocomposite hydrogels and adsorption of cationic crystal violet. *Carbohydrate Polymers*, ***98***(1), 358-365. DOI: 10.1016/j.carbpol.2013.05.096

Naidu, R., Biswas, B., Willett, I.R., Cribb, J., Singh, B.K., Nathanail, C.P., Coulon, F., Semple, K.T., Jones, K.C., Barclay, A. & Aitken, R.J. (2021). Chemical pollution: A growing peril and potential catastrophic risk to humanity. *Environment International*, ***156***, 106616. DOI: 10.1016/j.envint.2021.106616

Nwodika, C. & Onukwuli, D.O. (2017). Adsorption study of kinetics and equilibrium of basic dye on kola nut pod carbon. *Gazi University Journal of Science*, ***30***(4), 86-102.

Plaza, M., Santoyo, S., Jaime, L., Reina, G.G.B., Herrero, M., Señoráns, F.J. & Ibáñez, E. (2010). Screening for bioactive compounds from algae. *Journal of Pharmaceutical and Biomedical Analysis*, ***51***(2), 450-455. DOI: 10.1016/j.jpba.2009.03.016

Rueden, C., Dietz, C., Horn, M., Schindelin, J., Northan, B., Berthold, M. & Eliceiri, K. (2021). ImageJ Ops [Software]. https://imagej.net/Ops

Saravanan, A., Kumar, P.S., Jeevanantham, S., Karishma, S., Tajsabreen, B., Yaashikaa, P.R. & Reshma, B. (2021). Effective water/wastewater treatment methodologies for toxic pollutants removal: Processes and applications towards sustainable development. *Chemosphere*, ***280***, 130595. DOI: 10.1016/j.chemosphere.2021.130595

Ścieszka, S. & Klewicka, E. (2019). Algae in food: A general review. *Critical Reviews in Food Science and Nutrition*, ***59***(21), 3538-3547.

Shah, S.A.A., Hassan, S.S.U., Bungau, S., Si, Y., Xu, H., Rahman, M.H., Behl, T., Gitea, D., Pavel, F.M., Aron, R.A.C., Pasca, B. & Nemeth, S. (2020). Chemically diverse and biologically active secondary metabolites from marine Phylum chlorophyta. *Marine Drugs*, ***18***(10), 493. DOI: 10.3390/md18100493

Shojaei, T.R., Soltani, S. & Derakhshani, M. (2022). Synthesis, properties, and biomedical applications of inorganic bionanomaterials. In: Barhoum A., Danquah, M.K. (Ed), *Fundamentals of bionanomaterials*, 139-174p. Elsevier, Netherlands.

Sulaiman, S., Azis, R.A.S., Ismail, I., Man, H.C., Yusof, K.F.M., Abba, M.U. & Katibi, K.K. (2021). Adsorptive removal of copper (II) ions from aqueous solution using a magnetite nano-adsorbent from mill scale waste: synthesis, characterization, adsorption and kinetic modeling studies. *Nanoscale Research Letters*, ***16***, 1-17. DOI: 10.1186/s11671-021-03622-y

Thapa, S., Bharti, A. & Prasanna, R. (2017). Algal biofilms and their biotechnological significance. In: Rastogi, R.P., Madamwar, D. Pandey, A. (Ed), *Algal Green Chemistry*, 285-303p. Elsiever, Netherlands.

Tripathi, S., Sanjeevi, R., Anuradha, J., Chauhan, D.S. & Rathoure, A.K. (2022). Nano-bioremediation: nanotechnology and bioremediation. In: Khosrow, M. (Ed*), Research Anthology on Emerging Techniques in Environmental Remediation*, 135-149p. IGI Global.

Vázquez-Núñez, E., Molina-Guerrero, C.E., Peña-Castro, J. M., Fernández-Luqueño, F. & de la Rosa-Álvarez, M. (2020). Use of nanotechnology for the bioremediation of contaminants: A review, *Processes*, ***8***(7), 826. DOI: 10.3390/pr8070826

Wang, C.Y., Zhu, G.M., Chen, Z.Y. & Lin, Z.G. (2002). The preparation of magnetite Fe3O4 and its morphology control by a novel arc-electrodeposition method. *Materials Research*

Bulletin, ***37***(15), 2525-2529. DOI: 10.1016/S0025-5408(01)00787-5

Westra, L., Miller, P., Karr, J.R., Rees, W.E. & Ulanowicz, R.E. (2000). Ecological integrity and the aims of the Global Integrity Project. In: Pimentel, D., Westra, L., Noss R.F., (Ed), *Ecological Integrity: Integrating Environment, Conservation and Health*, 19-41p., Island Press, Washington, DC, USA.

Yusefi, M., Shameli, K., Rasit, A.R., Pang, S.W. & Teow, S.Y. (2020). Evaluating anticancer activity of plant-mediated synthesized iron oxide nanoparticles using *Punica granatum* fruit peel extract. *Journal of Molecular Structure*, ***1204***. DOI: 10.1016/j.molstruc.2019.127539